Supporting Information

Biodegradable fluorescent nanoparticles for endoscopic detection of colorectal carcinogenesis

*Author(s), and Corresponding Author(s)**
Stephan Rogalla, Krzysztof Flisikowski, Dimitris Gorpas, Aaron T. Mayer, Tatiana Flisikowska, Michael J. Mandella, Xiaopeng Ma, Kerriann M. Casey, Stephen A. Felt, Dieter Saur, Vasilis Ntziachristos, Angelika Schnieke, Christopher H. Contag, Sanjiv S. Gambhir*, and Stefan Harmsen**

Dr. S. Rogalla, A. T. Mayer, Dr. M.J. Mandella, Prof. S. S. Gambhir, Dr. S. Harmsen
Molecular Imaging Program at Stanford University (MIPS)
Department of Radiology
Stanford University School of Medicine
Stanford, CA 94305, USA
E-mail: sgambhir@stanford.edu; sharmsen@protonmail.com

A.T. Mayer and Prof. S. S. Gambhir
Department of Bioengineering
Department of Materials Science & Engineering
Stanford University
Stanford, CA 94305, USA

Dr. S. Rogalla
Department of Medicine (Gastroenterology & Hepatology)
Stanford University School of Medicine
Stanford, CA 94305, USA

Dr. K. Flisikowski, Dr. T. Flisikowska, Prof. A. Schnieke
Chair of Livestock Biotechnology
Technische Universität München
Liesel-Beckmann Str. 1
D-85354 Freising, Germany

Dr. X. Ma, Dr. D. Gorpas, Prof. V. Ntziachristos
Helmholtz Zentrum München
German Researcg Center for Environmental Health
Institute of Biological and Medical Imaging,
Ingolstädter Landstr. 1
D-85764, Neuherberg, Germany

Dr. X. Ma, Dr. D. Gorpas, Prof. V. Ntziachristos
Chair of Biological Imaging
TranslaTUM
Technische Universität München
Einsteinstr. 25
81675, Munich, Germany

Prof. K.M. Casey, Prof. S.A. Pelt
Department of Comparative Medicine
Stanford University School of Medicine
Stanford, CA 94305, USA

Prof. D. Saur
Department of Internal Medicine II
Klinikum Rechts der Isar
Technische Universität München
Ismaninger Str. 22
81675, Munich, Germany

Dr. M.J. Mandella, Prof. C.H. Contag
Institute for Quantitative Health Science and Engineering
Department of Biomedical Engineering
Michigan State University
775 Woodlot Dr.
East Lansing, MI 48824, USA
E-Mail: contagch@msu.edu

Dr. S. Rogalla and Dr. K. Flisikowski contributed equally.

Supporting Figures

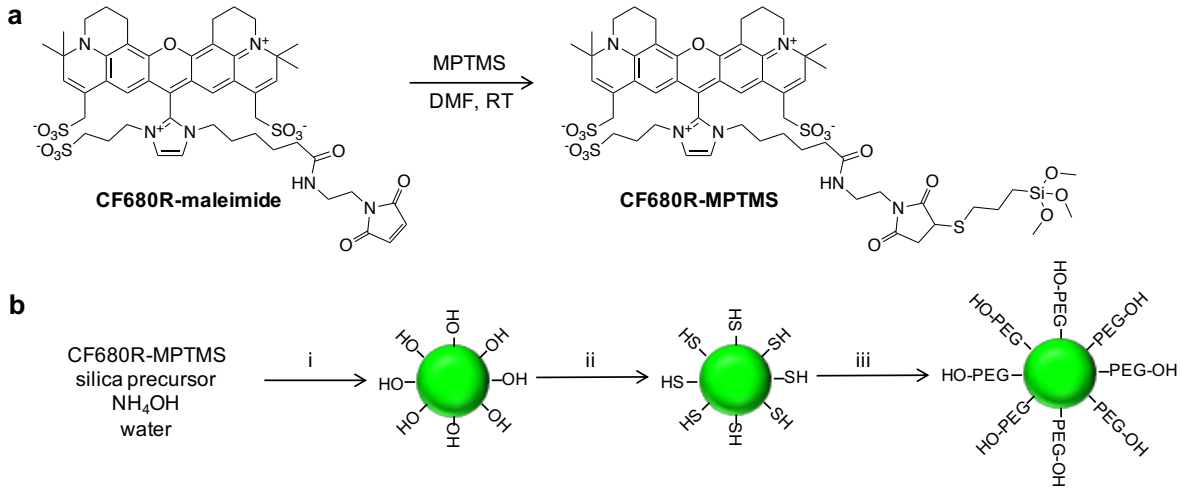

Figure S1. Fluorescent nanoparticle synthesis. a) CF680R-maleimide was reacted with (3-mercaptopropyl)trimethoxysilane (MPTMS) in a 1:2 molar ratio in *N*,*N*-dimethylformamide (DMF) to yield CF680R-MPTMS. b) Fluorescent silica nanoparticles were synthesized by reacting the silane-appended dye (concentration range CF680R-MPTMS: 0.19–3.0 μM, the silica precursor tetraethyl orthosilicate (TEOS; 4.5% (v/v)), 0.7% (v/v) ammonium hydroxide, and 8.0% (v/v) water in 2-propanol. Reaction conditions: *i*, 15 min, ambient conditions; *ii*, 5.5% (v/v) MPTMS, 0.5% (v/v) ammonium hydroxide in ethanol, while shaking (350 rpm) for 2-h at ambient conditions; *iii*, Excess maleimide-functionalized hydroxy-terminated polyethyleneglycol (PEG-OH; 3.4 kDa) in 10 mM 3-(*N*-morpholino)propanesulfonic acid (MOPS; pH 7.3), while shaking (350 rpm) for at least 2 h at ambient conditions.

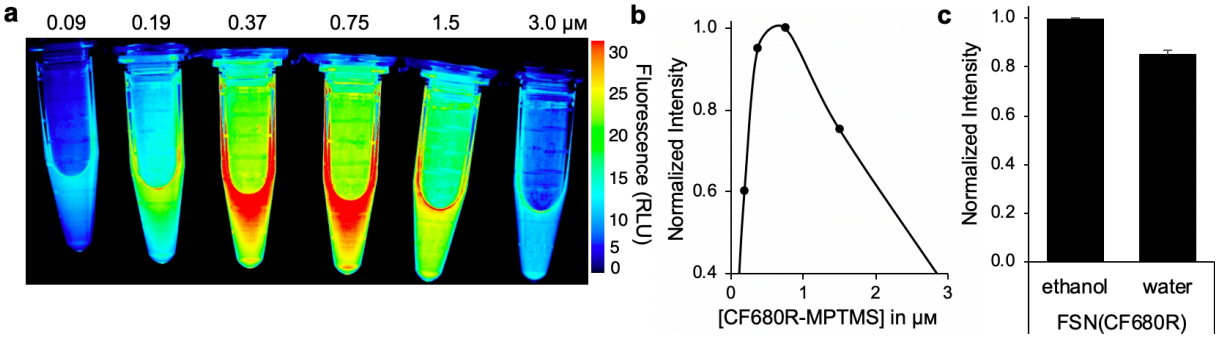

Figure S2. Effect of embedded-dye concentration and solvent on the fluorescence intensity of fluorescent silica nanoparticles. a) Effect of silane-appended CF680R concentration (in μM) on the fluorescence intensity of equimolar dispersions of as-synthesized fluorescent silica nanoparticles ($\lambda_{ex,em}$ = 680 nm, >700 nm). Fluorescence intensity is expressed as arbitrary units. b) Plot of normalized fluorescence intensity of the different as-synthesized fluorescent silica nanoparticles as a function of the silane-appended dye concentration present during nanoparticle synthesis. c) Effect of the solvent on the normalized fluorescence intensity of fluorescent silica nanoparticles dispersed in ethanol (EtOH) or water for 24 h. Data presented as mean (+SD).

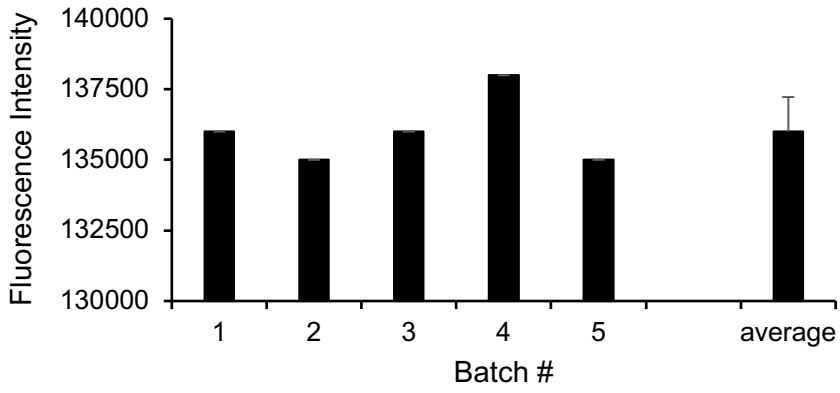

Figure S3. Reproducibility. Five different batches of FSNs were produced and NIRF of each batch was measured at 1 nM in EtOH ($\lambda_{ex,em}$ = 680 nm, >700 nm). Coefficient of variation is 0.9%. Fluorescence intensity is expressed as arbitrary units. Error bars represent standard deviation.

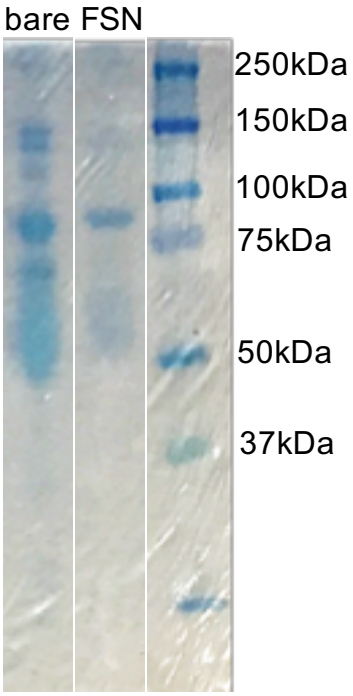

Figure S4. FSN protein adsorption. Bare (non-PEGylated) fluorescent silica nanoparticles and FSN grafted with hydroxy-terminated PEG (3.4 kDa) were incubated in 50% (w/v) human serum for 1 h at 37 °C. Next, the incubated nanoparticles were collected, washed, and redispersed in 10 μL water + 30 μL NuPage LDS sample buffer (ThermoFisher) containing 50 mM dithiothreitol (DTT). The samples were loaded on a 10-well NuPage 4–12% bis-tris PAGE gel and run at 100 V. The gels were stained with SimplyBlue SafeStain (ThermoFisher), washed with demineralized water, and photographed. As shown qualitatively, the protein stain in the FSN-lane was less intense than the bare-lane indicating that much less protein had bound to the FSNs.

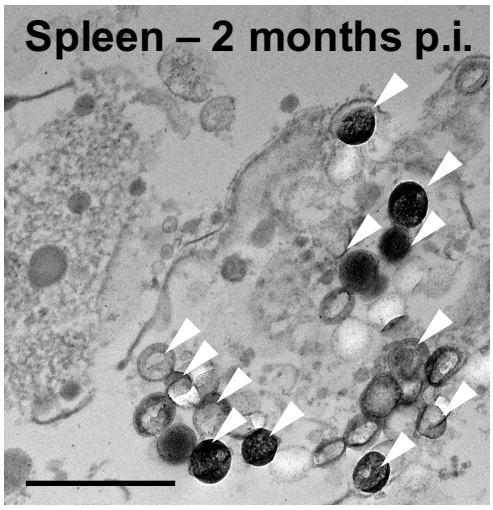

Figure S5. ***In vivo*** **biodegradation of FSNs.** Transmission electron microscopy (TEM) image of a spleen of the nude mouse that was sacrificed at 2 months post injection of FSN (30 fmol g^{-1}). At his time-point, the different stages of FSN degradation (etching from the inside, collapse, and dissolution; arrow heads) were fully captured *in situ*. Scale bar, 500 nm.

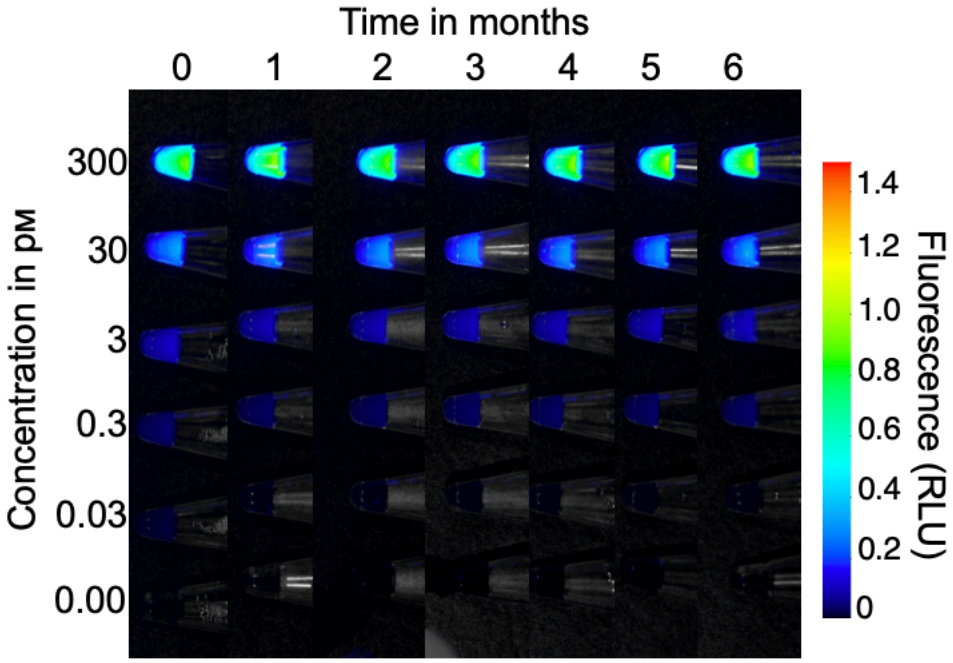

Figure S6. Photostability. The photostability of a standard concentration series (range 0.03 – 300 pM) of FSNs that was included in the biodegradation study. As such, the standard was imaged over the course of 6 months and subjected to ~200 exposures (1 s exposure time) during imaging on a Pearl Trilogy (Li-Cor). Coefficient of variations (CV) were less than 5% for all concentrations. Fluorescence intensity is expressed as arbitrary units.

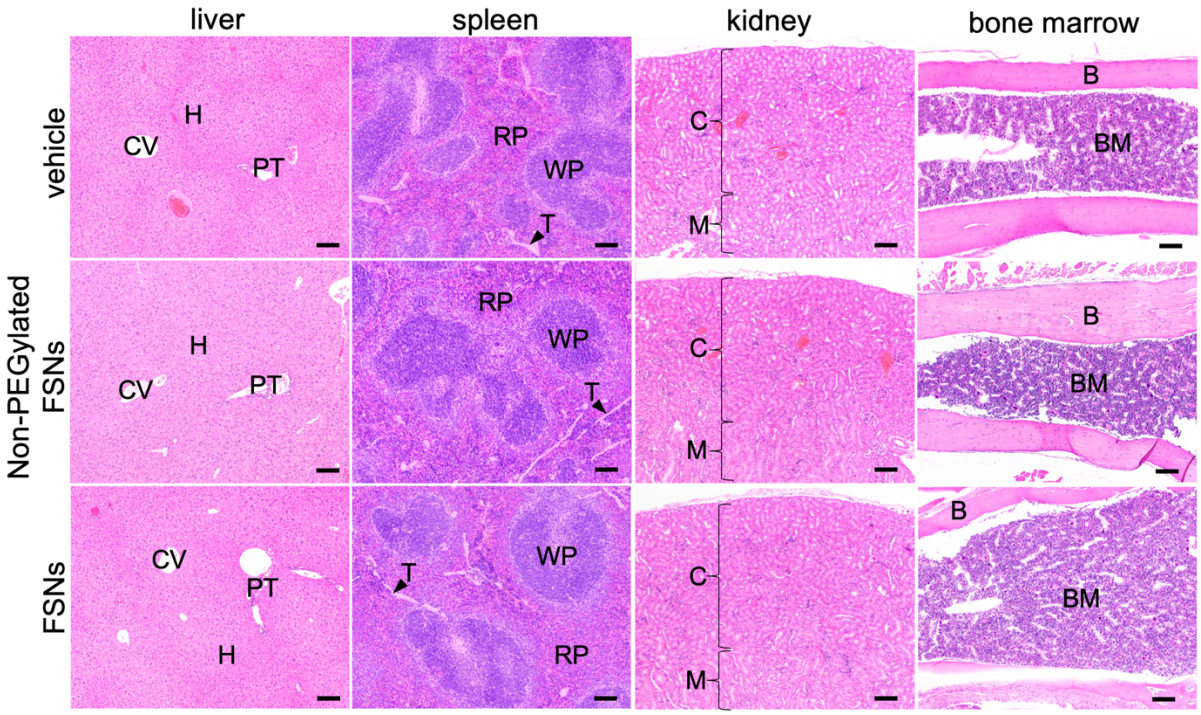

Figure S7. Histological assessment of organs following long-term FSN exposure. H&E sections of the mononuclear phagocyte system (MPS) organs (liver, spleen, and bone marrow) and kidneys following 6-months post tail-vein injection of FSNs (30 fmol g^{-1}) in nude mice (n=5). The organs of mice intravenously administered with non-PEGylated FSNs (30 fmol g^{-1}) or FSNs (30 fmol g^{-1}), were histologically indistinguishable from the organs of animals injected with a vehicle control (5% (w/v) D-glucose; D5W). No histologic abnormalities were noted in the liver (CV: central vein; PT: portal triad; H: hepatocytes), spleen (RP: red pulp; T: trabecula; WP: white pulp), kidney (C: cortex; M: medulla), or femoral bone marrow (B: femoral bone; BM: femoral bone marrow). Scale bar, 100 μm.

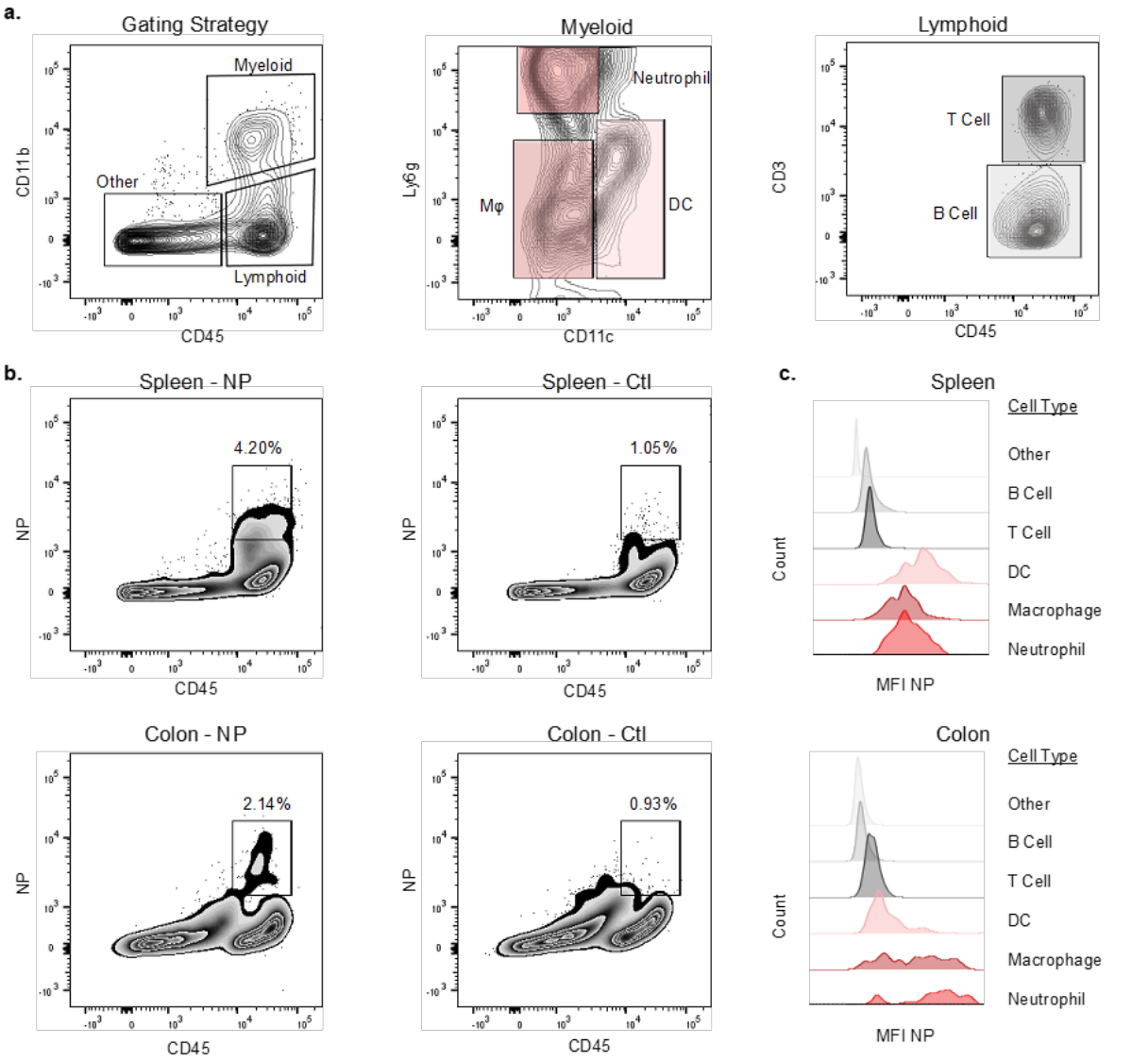

Figure S8. FSNs are preferentially taken up by phagocytic myeloid cells in the spleen and colon. a) Gating schematic – samples were first gated on singlets, live, cells prior to surface marker analysis. Cells were further gated on their expression of the cell surface markers CD45, CD11b, CD11c, CD3 and Ly6G to define myeloid and lymphoid cell subsets. b) FSN uptake within the spleen and colon of FSN treated animals compared to vehicle control D5W. c) Histograms (normalized to mode) of FSN uptake by various immune subpopulations. Other: $CD45^{-}CD11b^{-}$, B cell: $CD45^{+}CD11b^{-}CD3^{-}$, T cell: $CD45^{+}CD11b^{-}CD3^{+}$, Dendritic cell: $CD45^{+}CD11b^{+}CD11c^{+}$, macrophage: $CD45^{+}CD11b^{+}CD11c^{-}$, neutrophil: $CD45^{+}CD11b^{+}Ly6g^{+}CD11c^{-}$.

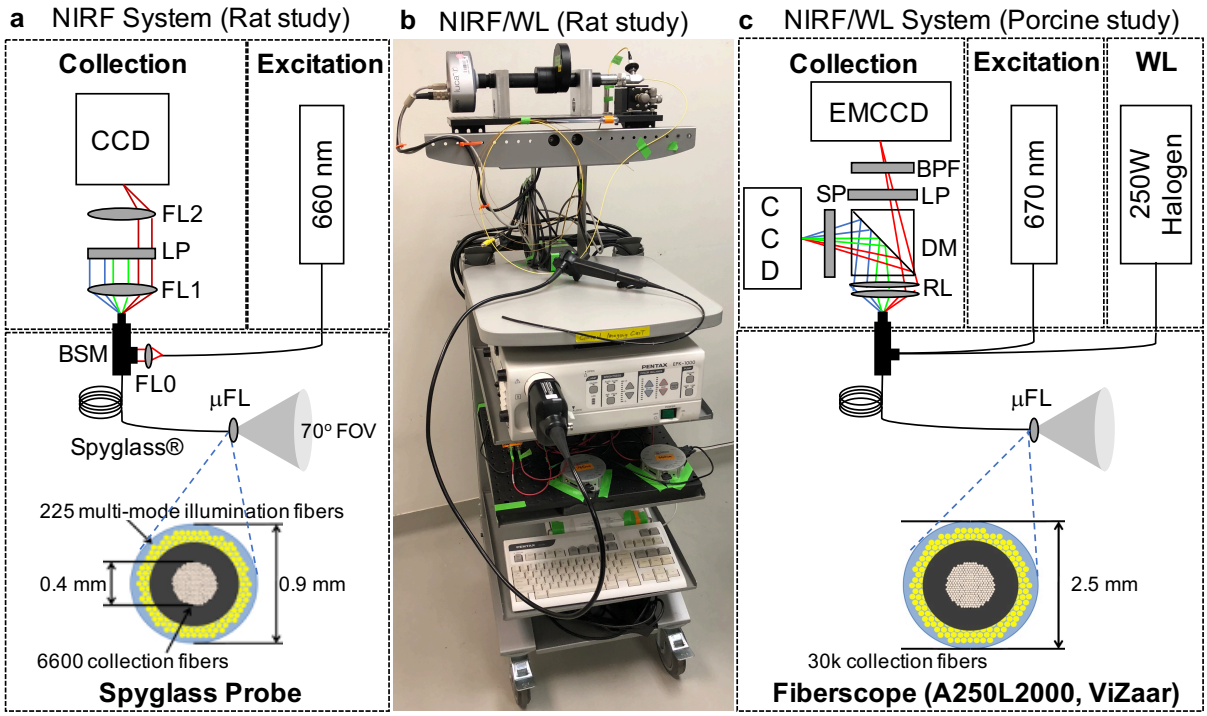

Figure S9. Dual-modal white light and NIR fluorescence fiberscope systems. a) Schematic of the NIRF endoscopy system that was used to perform the NIRF endoscopy in the rats. A 660-nm laser (IBeamSmart PT, Toptica Photonics AG, Gräfelfing, Germany) was coupled via a beam separation block (BSM) using a FL0 to a Spyglass fiberscope (Boston Scientific, Marlborough, MA), which has an outer diameter of ~0.9 mm and contains 225 multimode illumination fibers, 6600 collection fibers, and a 400-µm diameter lens (µFL), and provides a 70° field of view (FOV). Laser power output was measured to be 10 mW at the distal end. The collection fibers are focused (FL1: 20× Infinity-corrected Achromat Objective, F=9.0 mm, NA=0.4, WD=1.2 mm, Thorlabs #RMS20×; FL2: Infinity-corrected Tube Lens, Thorlabs #ITL200), filtered (LP: Long wavelength-pass filter 664 nm RazorEdge, LP02-664RU-25), and dispersed onto a 1-MPixel EMCCD camera (Luca R, Andor Technology, Belfast, UK). b) Photo of the custom-built NIRF/WL endoscopy system. The Spyglass fiberscope was fed into the instrument channel of a clinical white-light endoscopy system (EPK-1000, Pentax Medical, Montvale, NJ). The white-light endoscopy was recorded using GrabBee software and NIRF imaging was recorded using Solis software (Andor Technology). The combined WL/NIRF imaging was recorded using screen capturing software (Captivate, Adobe Inc, San Jose, CA). c) Schematic of the combined NIRF/WL endoscopy system that was used to perform the combined NIRF/WL endoscopy in the pigs. In brief, the imaging setup was designed to offer video-rate simultaneous color and near-infrared (NIR) fluorescence endoscopy. The system employs a multipurpose imaging fiber bundle with 30,000 coherently arranged individual fibers

(viZaar, Albstadt, Germany) achieving a 70° front viewing field of view. White-light illumination for color imaging was provided by a 250-W halogen lamp (KL-2500 LCD, Schott AG, Mainz, Germany), filtered by a 665 nm short-pass filter (FF01-665/SP-25, Semrock, Rochester, NY, United States) and NIRF excitation was achieved by a laser diode emitting at 670 nm (SLD1332V, Thorlabs, Newton, NJ, United States). A multibranched fiber optic bundle (Leoni FiberOptics, Neuhaus-Schierschnitz, Germany) realized simultaneous white-light illumination and NIRF excitation coupling to the flexible fiberscope. The images propagated through the fiberscope were relayed by a NIR achromatic doublet pair (RL: MAP10100100-B, Thorlabs) and separated by a dichroic mirror (DM: FF685-Di02, Semrock) into color and fluorescence channels. The color channel was filtered by a 665 nm short-pass filter (SP: FF01-665/SP-25, Semrock) for both cases and recorded by a 12-bit color charge-coupled device (CCD) camera (Pixelfly qe, PCO AG, Kelheim, Germany). NIRF detection spectral bandwidth was defined by a 685-nm long-pass filter (LP: FF01-685/LP-25, Semrock) followed by a 732/68-nm band-pass filter (BPF: FF01-732/68-25, Semrock) and recorded by an iXon electron multiplying charge-coupled device (EMCCD, DV897DCS-BV, Andor Technology, Belfast, Northern Ireland). The power at the distal end of the endoscope complied with the American National Standards Institute (ANSI) and the European Standards (EN) limits for the maximum permissive exposure in skin (19 mW/cm^2 for the 670-nm laser measured at distance <2 mm).

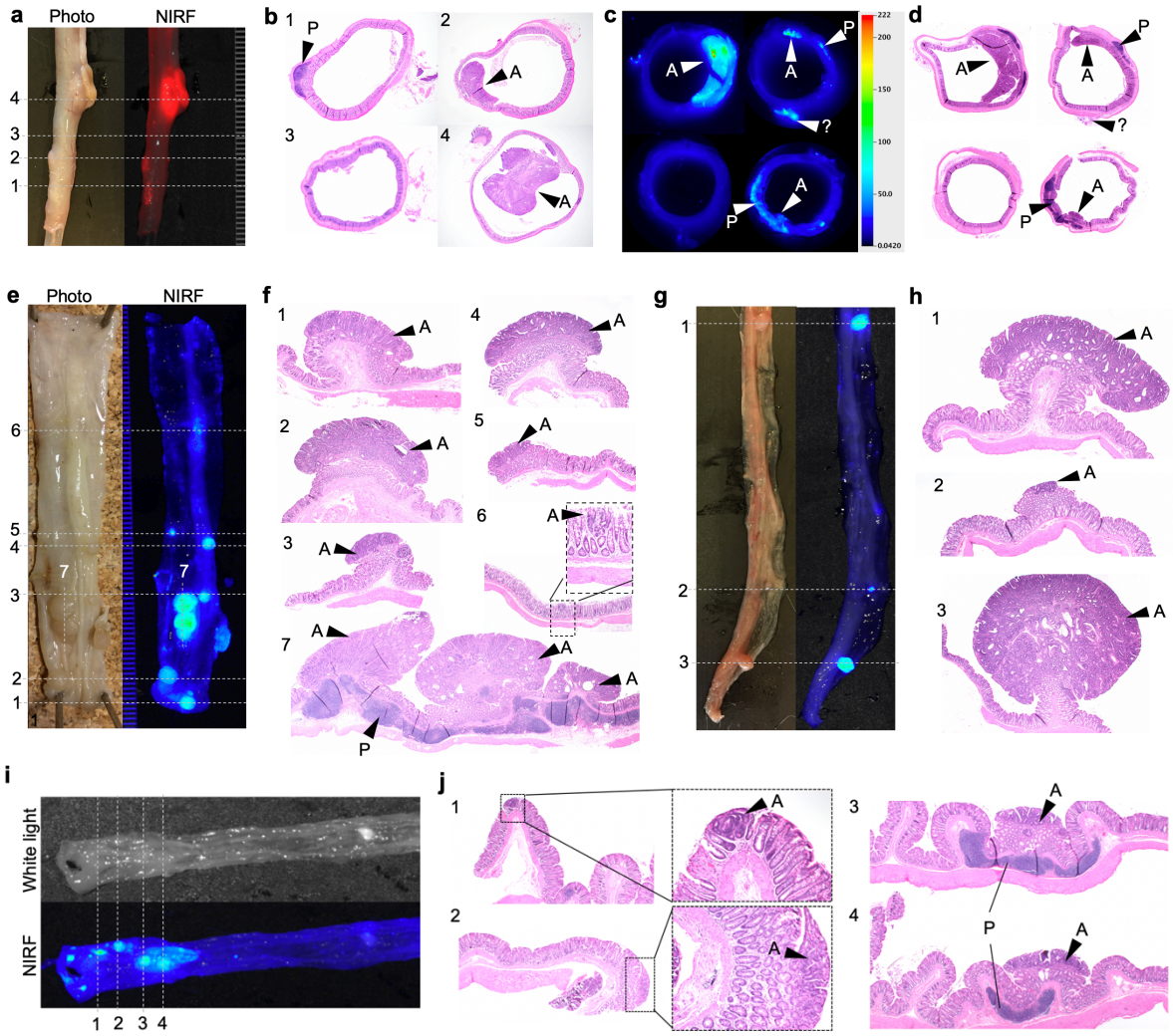

Figure S10. FSNs predominantly accumulate in colorectal adenomas of *Apc*$^{Pirc/+}$ rats intravenously injected with 30 fmol g^{-1} FSNs. a) Photo and NIRF images of the resected colon from rat 1. Grey lines (---) illustrate where the tissue was sectioned. b) H&E stained sections 1–4 correspond to 1) lymphoid tissue ('Peyer's patch'(P)), 2) adenoma (A), 3) normal colorectal mucosa, 4) adenoma. c) Fluorescent imaging of the paraffin-embedded colon sections and d) histology of random 5-µm thick sections of the resected colon of rat 2. e) Photo and NIRF images of the resected colon from rat 3. f) Histology of tissue sections 1–7. g) Photo and NIRF images of the resected colon from rat 4. h) Histology of tissue sections 1–3. i) White light and NIRF images of the resected colon from rat 5. j) Histology of tissue sections 1–4. See also **Table S1**.

Table S1. Performance of FSNs in *Apc*$^{Pirc/+}$ rats

Rat #	Fluorescent Lesions	Adenoma (A)	Peyer's patch (P)	unknown
1	3	2	1	0
2	6	3	2	1
3	10	9	1	0
4	3	3	0	0
5	5	4	1	0
Total	27	21	5	1